A 2D Coupled Electromagnetic, Thermal and Fluid Flow Model: Application to Layered Microwave Heat Exchangers

Ajit A. Mohekar[1], Joseph M. Gaone[2], Burt S. Tilley[1,2], and Vadim V. Yakovlev[2]
[1]Department of Mechanical Engineering, Worcester Polytechnic Institute, MA 01609, USA
[2]Department of Mathematical Sciences, Center for Industrial Mathematics and Statistics, Worcester Polytechnic Institute, Worcester, MA 01609, USA

***Abstract*—Development of efficient microwave heat exchangers requires complicated experimentation with processes of different physical nature. We describe here a 2D numerical model which can help study electromagnetic and thermal processes in the presence of fluid flows and design microwave heat exchangers based on layered structures. The model with no fluid flow captures the S- and SS-profiles of the power response curve, and is validated against the related 1D mathematical model; critical transition temperatures given by both models appear to be in satisfactory agreement. We show that thermal runaway is triggered by maximum temperatures in the system. A hydrodynamically fully developed Poiseuille flow is then introduced and steady state temperature profiles are found to be dependent on SS-curve. The results suggest a possibility of harnessing microwave energy.**

***Index Terms*—Microwave heating, multiphysics modeling, power response curve, thermal runaway**

I. Introduction

Traditional microwave (MW) heating systems are used in such applications as processing of food products, microwave-assisted chemistry, and high temperature treatment of materials [1], [2]. Relatively new devices are microwave heat exchangers (MHE), which are used in solar thermal collectors [3], wireless energy transmissions [4], and microwave thermal thrusters [5]. In addition to electromagnetic and heat transfer phenomena, MHE rely on effects involving fluid flows and thus require particularly extensive experimental developments. This raises demand on computational approaches and multiphysics models that are capable of adequately simulating all essential effects occurring in MHEs. Numerical models of continuous flow microwave heating [6], [7] are not applicable here because they are mainly focused on heating of continuously flowing fluid.

One peculiar phenomenon associated with MW processing of materials is thermal runaway, a non-linear phenomenon in which a small increase in power invokes a large increase in temperature. Thermal runaway was studied mostly experimentally [8], [9]. The theoretical description of thermal runaway was given for a single dielectric slab [10] and a three-layer geometry [11] in terms of a non-dimensional ratio of thermal losses to MW power represented the power response curve, otherwise called the S-curve. It shows how the steady-state temperature of the material depends on the MW power. This multi-valued curve implies that a system can reach different steady state temperatures when initial temperatures are different. The S-curve can also be interpreted as a balance between power absorbed and lost by the lossy material. A

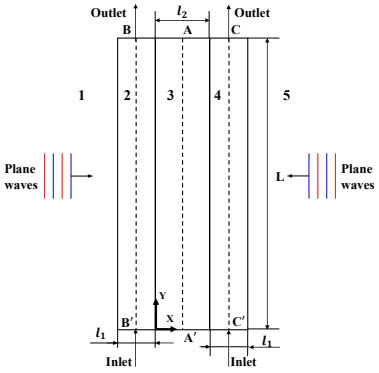

Fig. 1. Geometry of the three layered system subjected to electromagnetic heating (symmetric about AA'). Medium 1 and 5 are free space, layer 2 and 4 are lossless, layer 3 is a lossy dielectric.

branch of the S-curve is said to be stable when its slope is positive [11]. Thermal runaway occurs when the lossy material generates more heat than it loses. Recently, a mathematical model of a triple-layer laminate [12] showed that, for particular values of the layer's width and complex permittivity, the S-curve acquires another (third) stable branch and becomes the SS-curve. That opens a horizon for a new technique of keeping thermal runaway under control and efficiently converting electromagnetic energy into other usable forms of heat. While thermal runaway was computationally demonstrated in [13], numerical models reproducing the shapes of the power response curves have not been reported yet.

In this paper, we present a 2D numerical model developed in COMSOL Multiphysics for the three-layered structure imitating one of the MHE's basic setups. Initially, the model without fluid flow is validated against the related 1D mathematical model [12]. For this case, we demonstrate the behavior of a power response curve when spatial dependence of temperature is considered. We then incorporate coupling between electromagnetic, fluid flow, and heat transfer phenomena by introducing hydrodynamically fully developed Poiseuille fluid flow in region 2 and 4 along the Y-direction and visualize steady state temperature profiles that are dependent on initial temperature.

II. Computer Model

We consider a 2D, three-layered structure as shown in Fig. 1. This setup may be seen as a model of a MHE with absorbing (ceramic) layer surrounded by fluid channels. We

have plane waves incident from both sides with the assumption that the incoming waves are polarized along the Y-direction and traveling in the X-direction. Time average power density of the incident plane wave is

$$P_{av} = E_0^2/2\eta, \tag{1}$$

where E_0 is amplitude of electric field, and η is characteristic impedance of free space. In order to satisfy the resonance condition necessary to produce the SS-curve [12], we assume the frequency (f) to be 2.45 GHz, width of layers 2 and 4 as $3\lambda_2/4$ = 10.9 mm and width of layer 3 as $\lambda_3/2$ = 23.7 mm, where λ_2 and λ_3 are wavelengths of EM waves in medium 2 and 3, respectively; the length of the layers is L = 236.5 mm.

A. Governing equations

We construct a COMSOL model capable of solving a coupled system involving Helmholtz's, heat, and Navier-Stokes equations. We introduce non-dimensional variable $\tilde{E} = \vec{E}/E_0$, where $\vec{E}$ and $\tilde{E}$ are dimensional and non dimensional forms of the electric field, respectively. These equations are given by

$$\nabla^2\tilde{E}_j + k_0^2(\epsilon'_{rj} - i\frac{\sigma_j(T_j)}{\omega\epsilon_0})\tilde{E}_j = 0, \tag{2}$$

$$\frac{\partial T_j}{\partial t} + \vec{u_j}\cdot\nabla T_j = \alpha\nabla^2 T_j + \frac{Q_j}{\rho_j c_{p_j}}, \tag{3}$$

$$Q_j = \sigma_j(T_j)|E_0\tilde{E}_j|^2, \tag{4}$$

$$\frac{\partial\vec{u_j}}{\partial t} + \vec{u_j}\cdot\nabla u_j = -\frac{\nabla P_j}{\rho_j} + \nu_j\nabla^2\vec{u_j}, \tag{5}$$

$$\nabla\cdot\vec{u_j} = 0, \tag{6}$$

where $k_0 = \frac{\omega}{c}$ is wavenumber of free space, ω is angular frequency, c is speed of EM wave in free space, ϵ_0 is permittivity of free space, ϵ'_r is relative permittivity, T is temperature, $\sigma(T)$ is temperature dependent electrical conductivity, $\vec{u}$ is velocity, α is thermal diffusivity, Q is electromagnetic power loss density, ρc_p is volumetric heat capacity, P is pressure, and ν is kinematic viscosity. Subscript j represents region of the solution.

We solve (2) for $j = 1, ...5$, (3) for $j = 2, 3, 4$, (4) for $j = 3$, and (5) and (6) for $j = 2, 4$. For MW heating without fluid flow, $\vec{u_j} = 0$ for $j = 2, 3, 4$, the top and bottom boundaries of region 2, 3, and 4 are assumed to be thermally insulated. When fluid flow is considered, $\vec{u_2}, \vec{u_4}$ are non-zero and $\vec{u_3}$ is zero, pressure and temperature at the inlet in region 2 and 4 are 0.5 Pa at 300 K, respectively, the outlets in region 2 and 4 are thermally insulated and maintained at zero pressure, the top and bottom boundaries in region 3 are thermally insulated, and no slip conditions are applied at the external boundaries of channel 2 and 4. In both models, in order to neglect fringe effect at the corners of the geometry, we set normal component of gradient of the electric field to be zero at the top and bottom boundaries of region 2, 3, and 4, a symmetry condition is applied at AA', boundaries between region 1 and 2, 4 and 5 are exposed to ambient temperature of 300 K with heat transfer coefficient $h = 12.6\frac{W}{m^2K}$ undergoing Newton's law of cooling.

TABLE I
MATERIAL PROPERTIES

Medium	ϵ_r	$\sigma(T)[\frac{S}{m}]$	$\alpha[\frac{m^2}{s}]$	$\rho c_p[\frac{J}{m^3K}]$	$\nu[\frac{m^2}{s}]$
1, 5	1	0	-	-	-
2, 4	71	0	0.00137	435	0.0096
3	6.69	$0.001e^{\left[\frac{T-300}{100}\right]}$	0.00137	435	-

We also define the Biot number as $Bi = \frac{hl_2}{k_m}$, where k_m is the thermal conductivity of region 3.

B. Assumptions

Material properties used in computations below are chosen as shown in Table I. In particular, volumetric heat capacity is considered to be small to ensure that thermal runaway occurs at lower power levels and considerably reduce computational cost of sweeping over the large power range. Temperature dependent thermal properties are not considered in this model, but left for future developments. ϵ_r and μ_r are also assumed to be temperature independent. All the materials used are assumed non-magnetic ($\mu_r = 1$). In addition, only the middle layer (material 3) absorbs MW energy, and the outer layers (materials 1, 2, 4, and 5) are considered lossless.

C. Solver and convergence criteria

Selection of a solver in COMSOL Multiphysics strongly depends on degree of non-linearity. Helmholtz's and heat equations are coupled with each other via temperature dependent non-linear electrical conductivity, which has been shown to increase exponentially with the temperatures [14] for many dielectric materials. Depending on initial guess, while solving non-linear steady state problems, COMSOL's nonlinear steady state Newton-Raphson solver can fail to converge to desired solution. As temperature is a multi-valued function, initial guess is uncertain, therefore, we use the time-dependent solver and steady state is assumed to be reached when absolute difference between average temperatures at previous and current time step falls below 10^{-6}.

D. Meshing

The geometry is discretized using triangular elements, whose maximum size S_j is given by the Nyquist criterion:

$$S_j < \frac{\lambda_j}{2} = \frac{c}{2f\sqrt{\mu'_{rj}\epsilon'_{rj}}},$$

where λ_j is wavelength of the EM wave in corresponding region j. For robustness, we used 10 elements per wavelength throughout the computational domain. Similar mesh settings have been proved satisfactory in [6], [7].

For solving nonlinear problems effectively, we use an adaptive time stepping algorithm. Depending on temporal gradients of the fields, it automatically adjusts time step taken by the solver. The larger the gradients, the smaller the time step is. Since the time required for EM wave propagation is small compared to time required for heat transfer and fluid flow, Helmholtz's equations are solved in frequency domain, and the time stepping algorithm is utilized when solving heat and Navier-Stokes equations.

III. Computational Results

A. Excluding fluid flow

Fig. 2 shows the comparison of the power responses generated by the COMSOL model and the mathematical model of [12]. The mathematical model shows stable steady states as a solid line (branch AG and HM) and unstable states as a dashed line (branch GH). The transition between the lower and middle branches (Point G and H) do not occur at the same power level. This hysteresis is confirmed by the COMSOL model (Point C and F) through increasing power with an initial temperature at 300 K (path ABCDE) and then by decreasing power with an initial temperature of 750 K (path EDFBA). The mathematical model [12] assumes uniform heating in Y as does the COMSOL model, but it applies asymptotics to a thin domain resulting in a time dependent ordinary differential equation of average temperature uniform in the X-direction. In contrast, the COMSOL model captures the temperature variation along X.

In order to investigate the reason behind differences seen in power response curves produced by the COMSOL and mathematical models, we apply the conservation of energy principle to the system at steady state, and find that

$$\int_0^{l_2} \frac{1}{2}|E_0^2 \tilde{E}_3(T_3)|^2 \sigma_3(T_3) dx = 2h(\tilde{T}_2 - T_A), \tag{7}$$

where $\tilde{T}_2$ is surface temperature at $X = -l_1$, $T_3(x)$ is temperature profile in region 3, and l_1 and l_2 are the widths of layer 2 and 3 respectively. For the COMSOL model, from (1) and (7), input power density can be written as

$$P_1 = \frac{2h(\tilde{T}_2 - T_A)}{\eta \int_0^{l_2} |\tilde{E}_3(T_3(x))|^2 \sigma_3(T_3(x)) dx}. \tag{8}$$

Similarly, for the mathematical model, (1) and (7) can be simplified in terms of input power density as

$$P_2 = \frac{2h(\bar{T}_s - T_A)}{\eta |\tilde{E}_3(\bar{T}_s)|^2 \sigma_3(\bar{T}_s) l_2}, \tag{9}$$

where $\bar{T}_s$ is average steady state temperature in the model [12]. From (8) and (9), we can say that

$$P_2 - P_1 = \frac{2h(\bar{T}_s - \tilde{T}_2) - P_2 P^*}{\bar{P}_1}, \tag{10}$$

where

$$\bar{P}_1 = \eta \int_0^{l_2} |\tilde{E}_3(T_3(x))|^2 \sigma_3(T_3(x)) dx,$$

$$\bar{P}_2 = \eta |\tilde{E}_3(\bar{T}_s)|^2 \sigma_3(\bar{T}_s) l_2,$$

and

$$P^* = \bar{P}_2 - \bar{P}_1.$$

Numerical evaluation of (10) at the corresponding points on the SS-curve shown in Fig. 2 is given in Table II.

From the COMSOL model, we observe that thermal runaway is triggered by maximum temperatures in the lossy layer. Global temperatures increase rapidly as soon as the local maximum temperature reaches a critical temperature. Effect of spatial dependence of electric field and temperature can be understood from (10). We see that as we increase the Biot number by increasing h, $(\bar{T}_s - \tilde{T}_2)$ also increases, which then increases differences in power response curves. Fig. 3 shows the comparison of SS-curves for different values of the Biot number. At smaller Biot number, external surfaces will behave like a thermal insulator, which makes temperature profile nearly uniform in the X-direction. Therefore, as we decrease the Biot number, differences in the power response curves given by the COMSOL and mathematical models keep on decreasing. On the other hand, when the Biot number is large, spatial temperature variation becomes important, therefore, differences in power responses increase. It is observed that for increasing values of the Biot number, critical transition power also increases, but transition temperature remains the same.

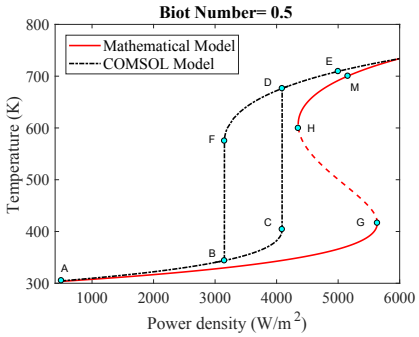

Fig. 2. Comparison of low power regions of power response curves in the considered structure. Temperatures at points C, G, F, and H are 413.5 K, 416.4 K, 574.6 K, and 606.6 K respectively.

TABLE II
Comparison of Critical Transition Powers

	Observed power density $[W/m^2]$	Observed $(P_2 - P_1)$ $[W/m^2]$	Calculated $(P_2 - P_1)$ $[W/m^2]$
Point C	P_1= 4088	1548	1548.55
Point G	P_2= 5636		
Point F	P_1= 3152	1199	1200.41
Point H	P_2= 4351		

We calculate the thermal energy in the system at steady state at critical temperature for both the COMSOL and mathematical models as

$$U = \int_V \rho c_p T dV.$$

The difference between the thermal energy levels at point G and C is 7.226 J. The model [12], which averages temperatures in the X-direction, has more thermal energy when the system is at critical temperature, thus a higher MW power is needed to reach this energy level (power corresponding to point G).

Thermal runaway in spatially dependent problems is driven by maximum temperatures in the lossy ceramic. The advantage of the COMSOL study is that it takes into account temperature variation in the X-direction due to the diffusive heat transfer to the exterior boundary of the laminate, unlike the model in

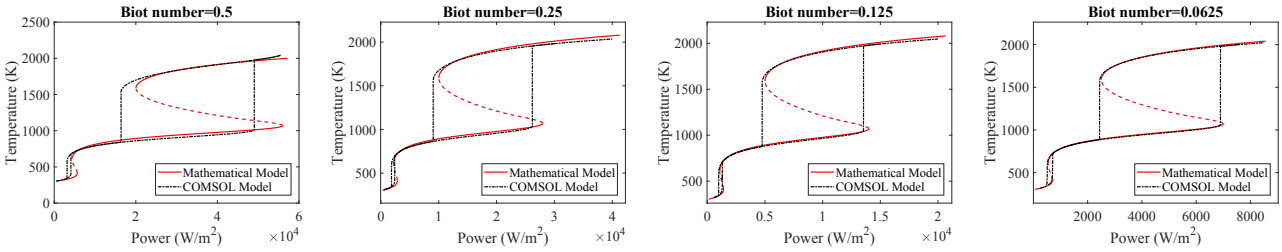

Fig. 3. Comparison of the SS curves produced by the COMSOL and mathematical models with different Biot numbers.

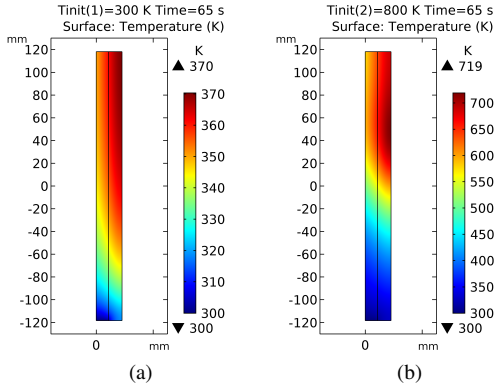

Fig. 4. Steady state temperature profiles when incident power was $3750W/m^2$ with initial temperature 300 K (a) and 800 K (b).

[12], does not need to use the uniform heating making it a more realistic model.

B. Including fluid flow

By keeping material parameters as shown in Table I, we introduce hydrodynamically fully developed Poiseuille flow in regions 2 and 4 in the Y-direction. Due to the fluid flow, temperature dependent electric field is no longer uniform in the Y-direction causing non-uniform heating. The difference between the models with and without fluid flow is the convective heat transfer between lossy layer and fluid. Fig. 4 shows two steady state temperature profiles when input power density is kept constant and initial temperature is changed from 300 K to 800 K. It is evident that heat convected by fluid when initial temperature was 800 K is much higher.

IV. Conclusion

We have developed a multiphysics model which is capable of producing SS-curves by considering local spatially dependent temperatures developed in the system. The model is validated by comparing its results with the related 1D mathematical model; critical transition temperatures given by both the models are reasonably close. We have found that thermal runaway is triggered by maximum temperatures in the system. Overall temperatures in the system increase rapidly when maximum temperature reaches the critical transition temperature. As thermal losses to the surrounding increase, critical power also increases, but critical temperature remains the same. The mathematical model, which averages temperatures in the X-direction, has more thermal energy when the system is at critical temperature, thus a higher MW power is needed to reach this energy level. Hydrodynamically fully developed Poiseuille flow has also been introduced, and temperature profiles are found to be dependent on the SS-curve. This result suggests a possibility of microwave energy harnessing. Future development of this work will include understanding effects of fluid flow on the power response curve.

Acknowledgment

The authors are grateful for the support from the Air Force Office of Scientific Research; Award FA9550-15-0476.

References

[1] A.C. Metaxas and R.J. Meredith, *Industrial Microwave Heating*, Peter Peregrinus Ltd., 1983.
[2] M. Willert-Porada, Ed., *Advances in Microwave and Radio Frequency Processing*, Springer, 2006.
[3] A. Jamar, Z.A.A. Majid, W.H. Azmi, M. Norhafana, and A.A. Razak, "A review of water heating system for solar energy applications", *Int. Commun. in Heat and Mass Transfer*, vol. 76, pp. 178-187, 2016.
[4] B. Jawdat, B. Hoff, M. Hilario, A. Baros, P. Pelletier, T. Sabo, and F. Dynys, "Composite ceramics for power beaming", In *2017 IEEE Wireless Power Transfer Conference*, 978-1-5090-4595-3/17.
[5] K.L. Parkin, L.D. DiDomenico, and F.E. Culick,"The microwave thermal thruster concept", In: *2nd Intern. Symp. on Beamed Energy Propulsion*, pp. 418-429, 2004, 0-7354-0175-6/04.
[6] D.A. Salvi, D. Boldor, G.M. Aita, and C.M Sabliov, "COMSOL multiphysics model for continuous flow microwave heating of liquids", *J. of Food Engineering*, vol. 104, no. 3, pp. 422-429, 2011.
[7] D. Salvi, D. Boldor, J. Ortego, G. Aita, and C. Sabliov, "Numerical modeling of continuous flow microwave heating: a critical comparison of COMSOL and ANSYS", *J. of Microwave Power and Electromag. Energy*, vol. 44, no. 4, pp. 187-197, 2010.
[8] X. Wu, *Experimental and Theoretical Study of Microwave Heating of Thermal Runaway Materials*, Ph.D. Thesis, Virginia Polytechnic Institute and State University, 2002.
[9] M. Chandran, V.B. Neculaes, D. Brisco, S. Katz, J. Schoonover, and L. Cretegny, "Experimental and numerical studies of microwave power redistribution during thermal runaway", *J. of Applied Physics*, vol. 114, no. 20, p. 204-904, 2013.
[10] G. Kriegsmann, "Themal runaway in microwave heated ceramic: a one-dimensional model", *J. of Applied Physics*, vol. 71, no. 4, pp. 1960-1966, 1992.
[11] J. Pelesko, G. Kriegsmann, "Microwave heating of ceramic laminates", *J. of Engineering Math.*, vol. 32, no. 1, pp. 1-8, 1997.
[12] J.M. Gaone, B.S. Tilley, and V.V. Yakovlev, "Permittivity-based control of thermal runaway in a triple-layer laminate", In: *IEEE MTT-S Intern. Microwave Symp. Dig. (Honolulu, HI, June 2017)*, 978-1-5090-6360-4.
[13] V.V. Yakovlev, S.M. Allan, M.L. Fall, and H.S. Shulman, "Computational study of thermal runaway in microwave processing of zirconia," *Microwave and RF Power Applications*, J. Tao, Ed., Cepatues Editions, 2011, pp. 303-306.
[14] J.M. Hill and M.J. Jennings, "Formulation of model equations for heating by microwave radiation," *Applied Math. Modelling*, vol. 17, no. 7, pp. 369-379, 1993.